

# Spontaneous layering and power-law order in the three-dimensional fully-packed hard-plate lattice gas.

Geet Rakala,<sup>1,\*</sup> Dipanjan Mandal,<sup>2,†</sup> Soham Biswas,<sup>3</sup> Kedar Damle,<sup>4,‡</sup> Deepak Dhar,<sup>5,§</sup> and R. Rajesh<sup>6,7,¶</sup>

<sup>1</sup>*Okinawa Institute of Science and Technology, 1919-1 Tancha, Onna-son, Kunigami-gun, Okinawa-ken, Japan*

<sup>2</sup>*Department of Physics, University of Warwick, Coventry CV4 7AL, United Kingdom*

<sup>3</sup>*Departamento de Fisica, Universidad de Guadalajara, Guadalajara, Jalisco, Mexico*

<sup>4</sup>*Department of Theoretical Physics, Tata Institute of Fundamental Research, Mumbai 400005, India*

<sup>5</sup>*Indian Institute of Science Education and Research,*

*Dr. Homi Bhabha Road, Pashan, Pune 411008, India*

<sup>6</sup>*The Institute of Mathematical Sciences, C.I.T. Campus, Taramani, Chennai 600113, India*

<sup>7</sup>*Homi Bhabha National Institute, Training School Complex, Anushakti Nagar, Mumbai 400094, India*

We study the phase diagram of fully packed hard plates on a cubic lattice. Each plate covers the four corner vertices of a plaquette, and each vertex of the lattice is covered by exactly one plaquette. We consider the general case with fugacities  $s_\mu$  for plates whose normal is the  $\mu$  direction ( $\mu = x, y, z$ ). At and close to the isotropic point, we find, consistent with previous work, a phase with long-range sublattice order. When two of the fugacities  $s_{\mu_1}$  and  $s_{\mu_2}$  are comparable, and the third fugacity  $s_{\mu_3}$  is much smaller, we find a spontaneously-layered phase with  $Z_2$  symmetry breaking of lattice-translation symmetry in the  $\mu_3^{\text{th}}$  direction. In this phase, the system breaks into layers of width two normal to the  $\mu_3$  axis, with only a small fraction of plates lying between layers. In the opposite limit, with  $\mu_3 \gg \mu_1 \sim \mu_2$ , we find a phase with long-range columnar order, corresponding to simultaneous  $Z_2$  symmetry breaking of lattice translation symmetry in directions  $\mu_1$  and  $\mu_2$ . The spontaneously-layered phases display critical behaviour, with power-law decay of correlations in the  $\mu_1$  and  $\mu_2$  directions, and represent examples of ‘floating phases’ discussed earlier in the context of coupled Luttinger liquids and quasi-two-dimensional classical systems. We ascribe this remarkable behaviour to the constrained mobility of defects in this phase, and develop a coarse-grained effective field theoretical understanding of the stability of power-law order in this unusual three-dimensional floating phase.

## I. INTRODUCTION

Fully-packed dimer models have been studied for several decades. On the one hand, they provide fascinating examples of entropically-driven ordering, closely analogous to Villain’s “order-by-disorder” phenomena in frustrated magnets [1]. On the other hand, on bipartite lattices, they also host highly-correlated liquid phases [2]. These “Coulomb phases” admit a natural description in terms of an effective field theory polarization fields, constructed by coarse-graining a lattice-level description in which each fully-packed dimer configuration is mapped to a divergence-free vector field on links of the lattice [3, 4]. In the two-dimensional cases of square and honeycomb lattices, this effective field theory correctly describes [5–9] the power-law columnar ordered state of the fully-packed dimer model on these lattices. In the three-dimensional cases of the cubic and diamond lattice, this correctly predicts that the fully-packed dimer model on these bipartite lattice displays a Coulomb liquid phase with dipolar power-law correlations between the dimers [10].

From this perspective, it is natural to go from this fully-packed lattice gas of hard rods on links of a cubic

lattice to a fully-packed lattice gas of plates that each touch four sites of an elementary plaquette of the cubic lattice, with each site of the lattice touched by exactly one plate. The key question then is whether such a lattice gas displays correlated liquid phases that could be understood by thinking in terms of tensor-valued analogs of the polarization fields that describe fully-packed dimer configurations. This is a natural speculation since one may view each plate as a pair of parallel dimers on the corresponding plaquette, which translates to two antiparallel dipoles that form a quadrupole with zero net dipole moment. Such a liquid phase would control properties of the corresponding resonating plaquette liquid states of SU(4) magnets [11] in much the same way as the Coulomb liquid phase of the interacting two-dimensional dimer model provides a description of energy correlations of resonating short-range valence bond wavefunctions [12, 13] of SU(N) magnets [14]. Motivated perhaps by this natural line of thought, previous work [15] used Monte-Carlo simulations to study fully-packed hard plates on the cubic lattice, with equal fugacities for plates of all orientations. It was found however that fully-packed hard plates on the cubic lattice develop long-range sublattice order [15], instead of correlated liquid behaviour that could have been described by such a coarse-grained theory of fluctuating quadrupolar tensor fields.

Here, we explore the rich phase diagram of this fully-packed lattice gas of plates in the general case with three possibly-distinct fugacities  $s_\mu$  for “ $\mu$ -normal” plates, *i.e.*

\* [geet.rakala@oist.jp](mailto:geet.rakala@oist.jp)

† [dipanjan.mandal@warwick.ac.uk](mailto:dipanjan.mandal@warwick.ac.uk)

‡ [kedar@theory.tifr.res.in](mailto:kedar@theory.tifr.res.in)

§ [deepak@iiserpune.ac.in](mailto:deepak@iiserpune.ac.in)

¶ [r.rajesh@imsc.res.in](mailto:r.rajesh@imsc.res.in)

with normal in direction  $\mu$  ( $\mu = x, y, z$ ). At and close to the isotropic point, we find a phase with long-range sublattice order, *i.e.* with two-fold ( $Z_2$ ) symmetry breaking of lattice translation symmetry in all three directions, consistent with the previous results alluded to earlier. When two of the fugacities  $s_{\mu_1}$  and  $s_{\mu_2}$  are comparable, and the third fugacity  $s_{\mu_3}$  is much smaller, we find a spontaneously-layered phase with  $Z_2$  symmetry breaking of lattice-translation symmetry in the  $\mu_3^{\text{th}}$  direction. In this phase,  $\mu_1$ -normal and  $\mu_2$ -normal plates preferentially occupy either all the odd bilayers perpendicular to the  $\mu_3$  axis, or all even bilayers of this orientation. In the opposite limit, with  $\mu_3 \gg \mu_1 \sim \mu_2$ , we find a phase with long-range columnar order, corresponding to  $Z_2$  symmetry breaking of lattice translation symmetry in directions  $\mu_1$  and  $\mu_2$ . The layered phases display critical behaviour, with power-law fall-off of correlations in the  $\mu_1$  and  $\mu_2$  directions. These represent examples of ‘floating phases’ discussed earlier in the context of coupled Luttinger liquids and quasi-two-dimensional classical systems.

To understand the stability of this unusual phase, we develop a coarse-grained effective field-theoretical description that builds on a coarse-grained description earlier for mixtures of dimers and hard squares on the two-dimensional square lattice. This effective field theory leads us to identify the constrained and correlated mobility of defects in this layered phase as being the key to its stability. The mechanism that stabilizes this phase is thus closely related to the physics of fractonic phases that have attracted a great deal of attention recently. This mechanism for the stability of the layered phase also suggests that this lattice gas of hard plates is expected to have interesting behaviours in the presence of a small density of mobile holes, again due to the restricted mobility of holes in the low density limit. The effect of vacancies has been studied in a parallel work[16] and will be reported on separately.

The rest of this paper is organised as follows: In Sec. II we first describe our parametrization of the model, and the order parameters used to identify its phases. Using this language, we also provide an overview of the phase diagram that we obtain from our computations. Sec. III is devoted to a summary of our computational methods. In Sec. IV we present the computational evidence for the phase diagram described in Sec. II. Sec. V is devoted to a closer look at the unusual structure of correlations exhibited by the layered phase, and a brief sketch of a coarse-grained field-theoretical description of this phase.

## II. MODEL, PHASE DIAGRAM AND ORDER PARAMETERS.

As already outlined in the Introduction, we study a fully-packed lattice gas of “hard” plates that each touch all four sites of an elementary plaquette of the cubic lattice. In this fully-packed limit, each site of the lattice

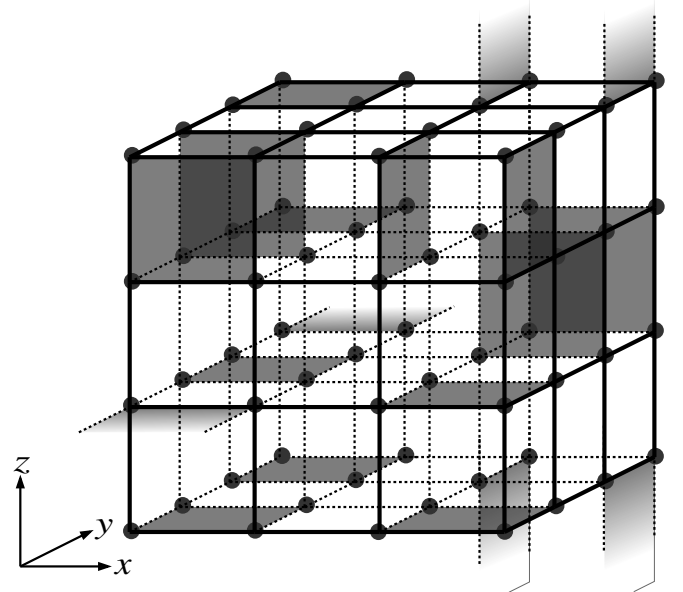


FIG. 1: A configuration of hard plates at full packing on the  $L = 4$  cubic lattice with periodic boundary conditions. Each plate touches exactly four sites of an elementary square plaquette of the cubic lattice, and each site is touched by exactly one such plate in the fully-packed case.

is touched by exactly one such plate. We consider the general case with fugacities  $s_\mu$  for ‘ $\mu$ -normal’ plates, *i.e.* with normal in direction  $\mu$  ( $\mu = x, y, z$ ). In place of the completely unambiguous but awkward terminology ‘ $\mu$ -normal plate(s)’ employed above, we adopt the less awkward usage ‘ $\mu$  plate(s)’ in the rest of this article. With periodic boundary conditions, the  $L^3$  sites of a  $L \times L \times L$  cubic lattice are covered by  $L^3/4$  hard plates in every such fully-packed configuration. We assign fugacities  $s_x$ ,  $s_y$  and  $s_z$  to  $x$ ,  $y$ , and  $z$  plates respectively, with all  $s_\mu \geq 0$ . We adopt the convention that these fugacities obey the constraint:

$$s_x + s_y + s_z = 3. \quad (1)$$

The partition function of the system is now given as

$$Z = \sum_C s_x^{n_x} s_y^{n_y} s_z^{n_z}, \quad (2)$$

where the sum is over all the fully-packed configurations of such a cubic lattice. An illustrative example of a configuration of the  $L = 4$  cubic lattice with periodic boundary conditions is shown in Fig. 1.

In our computational work, we use three different order parameters to quantitatively probe the nature of the various phases. These are the layering order parameter vector  $\vec{\mathcal{L}}$ , the columnar order parameter vector  $\vec{\mathcal{C}}$  and the scalar sublattice order parameter  $\omega$ . To define these, it

OP	x-columnar	y-columnar	z-columnar	x-layered	y-layered	z-layered	sublattice
$\mathcal{L}_x^2$	0	1	1	1	0	0	1
$\mathcal{L}_y^2$	1	0	1	0	1	0	1
$\mathcal{L}_z^2$	1	1	0	0	0	1	1
$\mathcal{C}_x^2$	1	0	0	0	0	0	1
$\mathcal{C}_y^2$	0	1	0	0	0	0	1
$\mathcal{C}_z^2$	0	0	1	0	0	0	1
$\omega^2$	0	0	0	0	0	0	1

TABLE I: Table showing various order parameters and the ordering patterns probed by them. 1 denotes a nonzero thermodynamic limit for a particular order parameter in that phase, while 0 indicates that it vanishes in the thermodynamic limit. The order parameters constructed using the alternate double-plate definitions behave in an entirely analogous manner.

is convenient to adopt a convention whereby each plate is assigned to a unique lattice site  $i$  as follows: Any plate touches four lattice sites. Except on ‘‘boundary plaquettes’’ created by the periodic boundary conditions, each plate is assigned to the site  $i$  (chosen from these four sites) that has the minimum value of all three cartesian coordinates  $x(i)$ ,  $y(i)$  and  $z(i)$ . On the wrapping plaquettes, this rule is modified in the obvious way for the cartesian coordinate(s) along which periodicity is being imposed. In the fully-packed limit, this implies that 1/4<sup>th</sup> of the lattice sites are assigned plates and the rest are touched by plates assigned to an adjacent lattice site.

Using this convention, we define two kinds of occupation variables on each site of the lattice: the single plate occupation  $\eta_\mu(i)$  takes a value 1 if a  $\mu$  plate is assigned to the site  $i$  and 0 otherwise; the double plate occupation  $\eta_{\mu\mu}(i)$  takes a value 1 if the corresponding single plate occupation  $\eta_\mu(i) = 1$  and there is another  $\mu$  plate present on the immediately adjacent plaquette in the  $+\hat{\mu}$  direction (here adjacency is defined taking into account the periodic boundary conditions).

The layering vectors  $\mathcal{L}_\mu$  and  $\mathcal{L}_{\mu\mu}$  are defined to measure translation symmetry breaking along direction  $\mu$ . For  $\mathcal{L}_\mu$ , we have

$$\mathcal{L}_x = \frac{1}{L^3} \sum_i l_x(i),$$

$$l_x(i) = (-1)^{x(i)} (\eta_x(i) + \eta_y(i) + \eta_z(i)), \quad (3)$$

and similarly for  $\mathcal{L}_y$  and  $\mathcal{L}_z$ . The layering vector  $\mathcal{L}_{\mu\mu}$  is defined in an entirely analogous manner, with all  $\eta_\gamma$  in the above replaced by  $\eta_{\gamma\gamma}$ . The corresponding definition of the columnar vectors  $\mathcal{C}_\mu$  and  $\mathcal{C}_{\mu\mu}$  is chosen to ensure that these vector order parameters are sensitive to translation symmetry breaking in the two cartesian directions perpendicular to  $\mu$ . For  $\mathcal{C}_\mu$  we have:

$$\mathcal{C}_x = \frac{1}{L^3} \sum_i c_x(i),$$

$$c_x = (-1)^{y(i)+z(i)} (\eta_x(i) + \eta_y(i) + \eta_z(i)), \quad (4)$$

and cyclically for the other components  $\mathcal{C}_y$  and  $\mathcal{C}_z$ . The

layering vector  $\mathcal{C}_{\mu\mu}$  is again defined as above, but with all  $\eta_\gamma$  replaced by  $\eta_{\gamma\gamma}$ .

In addition, we define the scalar sublattice order parameter  $\omega$  to measure the simultaneous breaking of translation invariance along all three directions:

$$\omega = 27(\mathcal{L}_x \mathcal{L}_y \mathcal{L}_z), \quad (5)$$

where the factor of 27 is simply a convenient convention. Note that this quantity, unlike the layering and columnar vectors, is not being defined as a sum over a scalar density defined locally on the lattice. Instead, it is simply the product of three components of the layering vector  $\mathcal{L}_\mu$ . This product is sensitive to the simultaneous breaking of lattice translation symmetry in all three directions of the cubic lattice, and hence probes the presence of sublattice order. For a convenient summary of the various order parameters and the ordering patterns they probe, see Table. I.

We choose this somewhat unconventional definition to finesse a curious difficulty that arises if one uses the seemingly more natural definition of a scalar sublattice order parameter

$$\phi = \frac{1}{L^3} \sum_i (-1)^{x(i)+y(i)+z(i)} (\eta_{xx}(i) + \eta_{yy}(i) + \eta_{zz}(i)). \quad (6)$$

Our results indicate that  $\langle \phi^2 \rangle$  defined in this way remains extremely small throughout the phase diagram, and cannot be used to draw any reliable conclusions. Why this is the case is not entirely clear. Since  $\omega$  can in any event be used to unambiguously detect the presence of sublattice order independent of this curious behaviour of  $\phi$ , we may safely side-step this difficulty as far as our results here are concerned. However, we emphasize that this behaviour of  $\phi$  is an interesting puzzle that deserves further study in follow-up work.

For each order parameter  $\mathcal{O}$ , we monitor the  $L$  dependence of  $\langle \mathcal{O}^2 \rangle$  to determine whether the phase in question is characterized by the corresponding long range ordering behaviour. Since our definitions of all the order parameters include a normalization by a factor of  $L^3$  to render

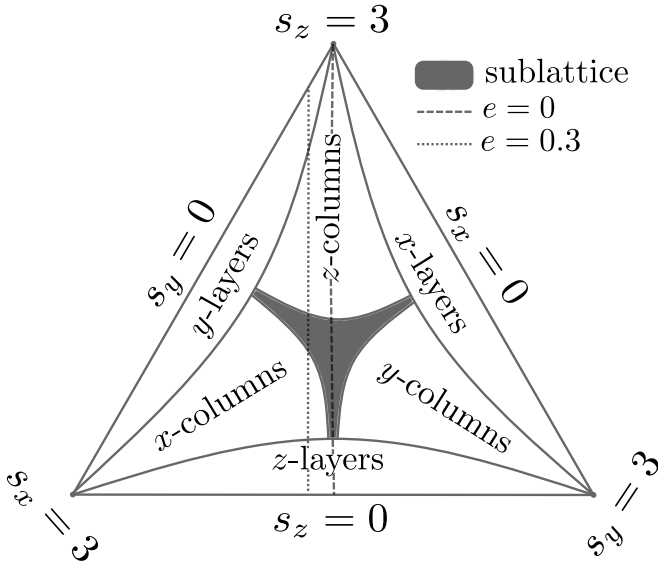


FIG. 2: A schematic of the phase diagram inside the fugacity triangle that represents the parameter space of the fully-packed hard square lattice gas. Note that the fugacities  $s_\mu$  ( $\mu = x, y, z$ ) satisfy  $s_x + s_y + s_z = 3$  in our convention. In this convention, the corners of the triangle correspond to the points  $s_x = 3, s_y = 3$  and  $s_z = 3$  respectively, while the sides correspond to the lines  $s_x = 0, s_y = 0$ , and  $s_z = 0$  respectively. The two cuts shown, corresponding to  $e = 0$  and  $e = 0.3$  (where  $e = s_x - s_y$ ), are the ones along which our most detailed results have been obtained. There are three kinds of phases: A sublattice-ordered phase, with lattice translation symmetry broken in all three Cartesian directions, layered phases with lattice translation symmetry broken only along one cartesian direction, and columnar ordered phases with lattice translation symmetry broken along two of the three cartesian directions.

it intensive,  $\langle \mathcal{O}^2 \rangle$  is expected to vanish as  $L^{-3}$  in the absence of long range order, tend to a nonzero limit in the presence of long range order, and vanish as  $L^{-(d-2+\eta)}$  with  $d = 3$  if it has an order parameter correlation function falling off as  $1/r^{d-2+\eta}$  with  $\eta < 2$ . Note however that  $\langle \mathcal{O}^2 \rangle$  cannot distinguish a power-law ordered phase with  $\eta > 2$  from a disordered phase, since  $\langle \mathcal{O}^2 \rangle \sim 1/L^3$  in both cases, but the two can still be distinguished by measuring the order parameter correlation function. Finally, it is also important to realize that  $\langle \omega^2 \rangle$  is expected to have a somewhat different fall-off in a phase without sublattice order: If the phase is a columnar ordered phase, one expects a  $1/L^3$  fall off, but a phase which is disordered in two cartesian directions and breaks lattice translation symmetry in only one direction is expected to display a  $1/L^6$  fall off of  $\langle \omega^2 \rangle$ . As we will see below, the layered phase that arises in our hard plate system has power-law order in the transverse directions. As a result, we expect  $\langle \omega^2 \rangle$  to display a power-law fall off with

exponent somewhat smaller than 6.

For each of these order parameters, we also monitor the Binder ratio  $U_{\mathcal{O}}$ :

$$U_{\mathcal{O}} = \frac{\langle \mathcal{O}^4 \rangle}{\langle \mathcal{O}^2 \rangle^2}. \quad (7)$$

Clearly, this ratio tends to unity in the thermodynamic limit of an ordered state. In a disordered state, it tends to a value larger than one, which depends on the number of independently fluctuating components that make up  $\mathcal{O}$ . Thus, the Binder ratio of a scalar order parameter tends to a limiting value of 3, while that of a two-component vector tends to 2, and so on.

The parameter space of this fully-packed lattice gas may be conveniently represented by an equilateral *fugacity triangle*, with the three vertices corresponding to  $s_x = 3, s_y = 3$  and  $s_z = 3$  respectively as shown in Fig. 2. The sides of this triangle then correspond to the  $s_x = 0, s_y = 0$  and  $s_z = 0$  lines. The center of mass of this triangle represents the isotropic point where  $s_x = s_y = s_z = 1$ . Clearly, the phase diagram represented within the equilateral triangle must have a three-fold permutation symmetry  $S_3$  about the center of the triangle. In our computations, we have used this fact to deduce the schematic structure of the phase diagram from results obtained along a few cuts through the interior of the triangle. A schematic of the phase diagram thus obtained is displayed in Fig. 2; also depicted are the two cuts along which we have obtained our most detailed results. A convenient way to summarize our findings along these two cuts is to plot the behaviour of the three components of the layering vector  $\vec{\mathcal{L}}$  along these cuts. This is shown in Fig. 3

As is clear from this phase diagram, we find a phase with long-range sublattice order at and close to the isotropic point, *i.e.* when all three fugacities are comparable to each other, and the corresponding densities are likewise comparable. This finding is consistent with a previous study of isotropic fully-packed plates, which found in favour of a sublattice-ordered state [15]. Our study allows us to go beyond this and study the competition between this sublattice ordered phase and the other two kinds of phases described above.

Indeed, when two of the fugacities  $s_{\mu_1}$  and  $s_{\mu_2}$  are comparable, and the third fugacity  $s_{\mu_3}$  is much smaller, we find a spontaneously-layered phase with  $Z_2$  symmetry breaking of lattice-translation symmetry in the  $\mu_3^{\text{th}}$  direction. In this phase,  $\mu_1$ -normal and  $\mu_2$ -normal plates preferentially occupy either all the odd bilayers perpendicular to the  $\mu_3$  axis, or all even bilayers of this orientation.

In the opposite limit, with  $\mu_3 \gg \mu_1 \sim \mu_2$ , we find a phase with long-range columnar order, corresponding to simultaneous  $Z_2$  symmetry breaking of lattice translation symmetry in directions  $\mu_1$  and  $\mu_2$ .

To probe the nature of the layered phase in more detail, we study the intra-layer and inter-layer correlation functions of the transverse components of the layering

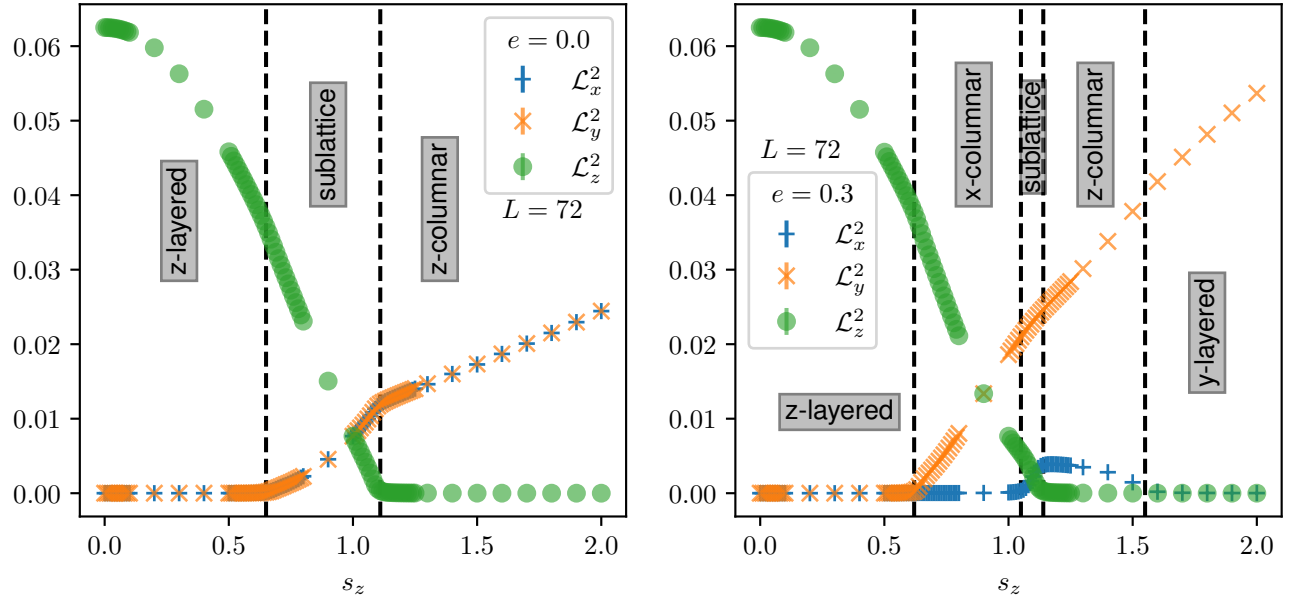


FIG. 3: The behaviour of the three different components of the layering vector  $\vec{\mathcal{L}}$  along the two cuts shown in Fig. 2 provides a convenient way to recognize at a glance the presence of sublattice ordered, columnar ordered, and layered phases in various parts of the phase diagram. The sublattice ordered phase is distinguished by nonzero mean square values for all three components of the layering vector. In a columnar ordered phase, two components of the layering vector have nonzero mean square values, while the mean square value of the third vanishes in the thermodynamic limit. In a layered phase, only one component of the layering vector has a nonzero mean square value.

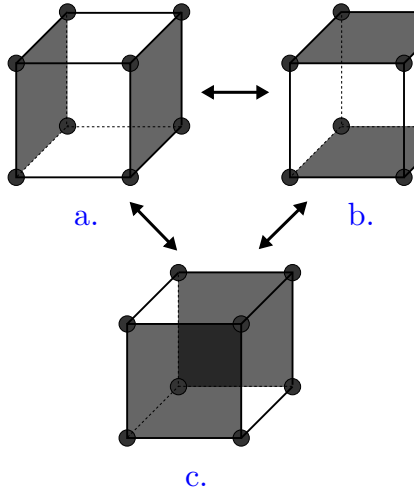


FIG. 4: Figure showing all the local moves in a ring exchange.

order parameter. To this end, we first define

$$l_{x\perp}(z) = \sum_{x,y} l_x(x, y, z),$$

$$l_{y\perp}(z) = \sum_{x,y} l_y(x, y, z). \quad (8)$$

In terms of  $l_{x\perp}$  and  $l_{y\perp}$ , we can now define

$$G(L, \Delta z) = \sum_z \langle (l_{x\perp}(z)l_{x\perp}(z + \Delta z) + l_{y\perp}(z)l_{y\perp}(z + \Delta z)) \rangle. \quad (9)$$

In what follows, we will denote  $G(z, \Delta z = 0)$  by simply  $G(L)$ , while keeping the second argument when it is nonzero. In principle, the sum over  $z$  in the definition of  $G(L, \Delta z)$  should be taken only over “occupied” bilayers, with the convention that all  $z$  plates are assigned to the occupied bilayers. However, we have checked that summing over all  $z$ , which is computationally simpler, gives qualitatively similar results, motivating the definition above. As an independent check on this way of looking at the intra-layer correlations, we have also measured the  $r$  dependence of  $g(r)$ , defined as the connected intra-layer correlation function of  $l_x$  and  $l_y$  within a single bilayer. Power-law columnar order, with  $g(r) \sim 1/r^\eta$  within a bilayer would give rise to  $G(L) \equiv G(L, \Delta z = 0) \sim 1/L^\eta$  for  $\eta < 2$ , while  $G(L) \sim 1/L^2$  for  $\eta > 2$ .

### III. COMPUTATIONAL METHODS

Our Monte Carlo simulations use a combination of local updates supplemented by a cluster algorithm to improve the equilibration and reduce autocorrelation times.

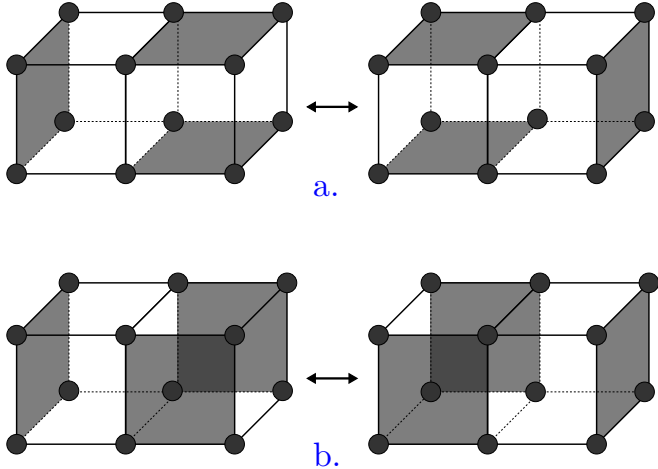


FIG. 5: Figure showing the local moves in a shift exchange.

We use two types of local updates: a *ring* exchange move, and a *shift* exchange:

*Ring exchange:* The ring exchange move, shown in Figure 4, relies on the fact that all eight vertices of an elementary cube can be touched by two plates that cover two opposite faces of the cube. There are three such “perfect covers” of any elementary cube. The idea is to try and exchange one such perfect cover of the cube for another perfect cover chosen with probabilities that satisfy detailed balance. To implement this, one randomly picks an elementary cube of the cubic lattice, and checks if it is of this “perfectly covered” or “flippable” type. If the answer is yes, then one looks up a previously constructed probability table listing the relative weights in the partition sum of the three different perfect covers of this cube. Using this probability table, one chooses transition probabilities with detailed balance, and replaces the original perfect cover with a fresh one. If a “no-bounce” solution of the detailed balance constraints is possible [17], then the final state is always one of the other two perfect covers. If the weight of one of the three perfect covers is larger than the sum of the other two, then a “no-bounce” solution is not possible [17], and there is a nonzero probability that the final state will be the same as the original perfect cover.

*Shift exchange:* The *shift* exchange starts by picking a random pair of adjacent elementary cubes of the lattice sharing a face with each other. Let the shared face have a normal in the  $\mu$  direction. If one of the elementary cubes is perfectly covered by a pair of  $\nu$  plates, where  $\nu \neq \mu$ , and the other elementary cube has its remaining four sites touched by a  $\mu$  plate, then the configurations of the two elementary cubes are interchanged (see Fig. 5). Since this does not change the orientation of the three plates involved, no probability table is needed, and this shift exchange can be carried out whenever the randomly chosen pair of adjacent elementary cubes host a configuration of this type.

To supplement these two updates and improve auto-correlation times of the Monte Carlo algorithm, particularly in the presence of periodic boundary conditions, one can supplement these basic local updates with two kinds of non-local updates. The first uses a transfer matrix method to update an entire one dimensional tube, keeping the rest of the configuration fixed. This generalizes the approach used previously for simulations of a mixture of hard squares and dimers in two dimensions [18]. The other is a cluster algorithm that generalizes the pocket cluster algorithm [19] used previously to study fully-packed dimer models. Here, we show results obtained using the second approach, *i.e.* using a generalization of the pocket cluster algorithm [19]. In parallel work [16] that studies the effects of vacancies on our fully-packed lattice gas, we use the alternate transfer matrix scheme [16].

In the cluster update scheme, we rely on the existence of  $\mathcal{O}(L)$  different reflection symmetries of the system, each of which square to the identity operation. For this to be the case, periodic boundary conditions are essential. To begin, a reflection is specified by picking a randomly chosen reflection plane. Six kinds of reflection planes, each perpendicular to one of the three cartesian directions and either containing sites of the lattice or bisecting bonds of the lattice, always define valid symmetry operations for general values of fugacities. Of these, we choose to use the  $3L$  planes that contain sites of the lattice. In addition, one can consider reflections about “diagonal” reflection planes, specified by a normal that lies either in the  $xy$  plane and makes an angle of  $\pm\pi/4$  with the  $x$  and  $y$  axis, or does the same in the  $yz$  or  $zx$  plane. These 6 kinds of additional reflections are all symmetries of the system only at the isotropic point when all the fugacities are equal. Elsewhere in the fugacity triangle, at most two of them are symmetries.

The cluster update begins by randomly choosing (with equal probability) one of the possible reflection symmetries of the system, say a reflection about the symmetry plane  $\mathcal{S}$ . In addition, a plate is chosen at random as the seed. Apart from the physical system, one constructs a “pocket lattice”, which is empty to begin with. The seed plate is acted on by the reflection operation corresponding to the randomly chosen symmetry plane  $\mathcal{S}$ . This can change its location, and, possibly its orientation too. Thus transformed, the plate is moved to the pocket lattice and placed in its possibly new location (and possibly new orientation). Next, this transformed plate is moved back to the physical lattice so that it now occupies a transformed location with a transformed orientation in the physical lattice. As a result, it touches some other plates in the physical lattice. These other plates are now removed from the physical lattice, transformed according to the symmetry operation  $\mathcal{S}$ , and moved to the pocket lattice.

The rest of the update consists of repeating this process until the pocket lattice is empty. In other words, at each step, we take a plate from the pocket lattice,

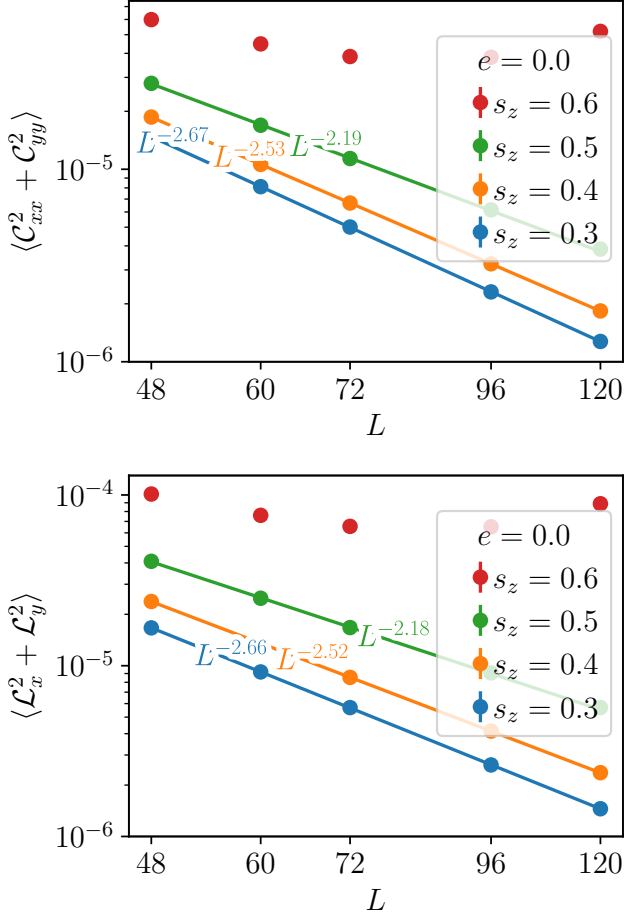


FIG. 6:  $\langle C_{xx}^2 + C_{yy}^2 \rangle$  (top) and  $\langle L_x^2 + L_y^2 \rangle$  (bottom) as a function of  $L$  on the  $e = 0$  cut across the  $z$  layered to sublattice order transition for  $s_z \in [0.3, 0.6]$ .

move it back to the physical lattice so that it occupies a transformed location with a transformed orientation, and then remove the plates it touches in the physical lattice, transform them, and move them to the pocket lattice. Once the pocket lattice is emptied at the end of this process, the physical lattice again has a fully-packed configuration that does not violate any constraints. This new configuration can be accepted with probability one since the weight of the configuration has not changed in this process.

We simulate the system using a combination of these local and cluster updates. Each Monte Carlo step (MCS) involves  $L^3$  number of ring exchanges,  $L^3$  shift exchanges in the  $\hat{x}$ ,  $\hat{y}$  and  $\hat{z}$  directions each, and a number of cluster updates, each involving a randomly chosen symmetry plane and a random seed plate (this number is chosen to ensure that a total of  $\mathcal{O}(L^3)$  plates are involved in these cluster updates as a whole). The Monte Carlo routine was tested against exact enumeration on a  $4 \times 4 \times 2$  periodic lattice with fully-packed hard plates using Martin's backtracking algorithm[20].

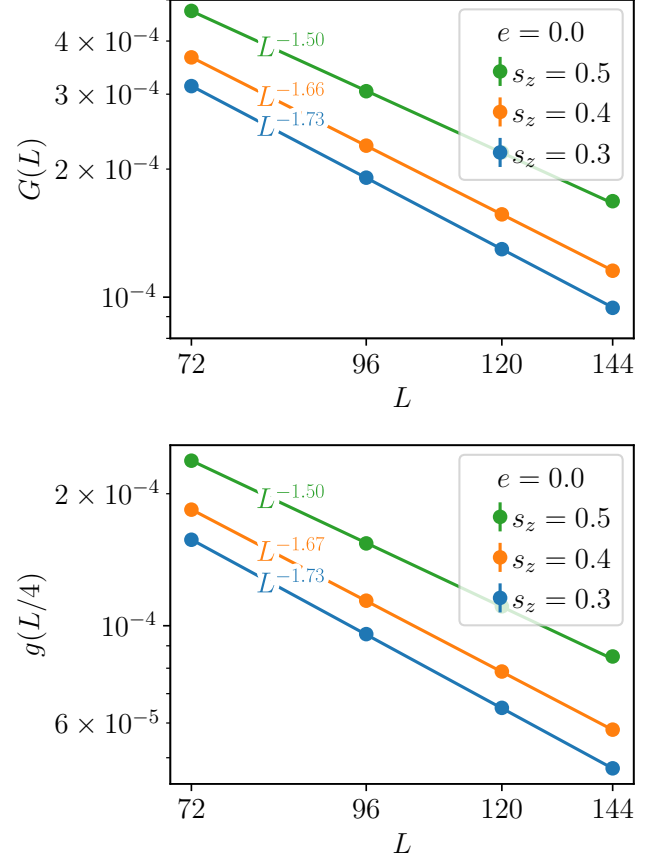


FIG. 7:  $G(L)$  (top) and  $g(L/4)$  (bottom) as a function of  $L$  on the  $e = 0$  cut for  $s_z \in [0.3, 0.5]$ .

At each set of fugacity parameters, simulations were carried out on lattices of size  $L = 48, 60, 72, 96$  and  $120$ . Simulations at each set of parameter values involved at least 10 random initial seeds, a warm-up of  $2 \times 10^5$  MCS for each seed followed by a run length of  $2 \times 10^6$  MCS for each seed, with measurements being taken at every two MCS.  $10^3$  such measurements were binned to create one notionally independent measurement. Error bars were estimated by re-binning these notionally independent measurements in sets of 5, 50 and 100 and using the re-binned estimators to calculate three different estimates of the statistical error. The actual error bar assigned to each data point was taken to be the maximum of these three estimates. Independent simulations at each set of parameter values were parallelised using GNU parallel.

#### IV. COMPUTATIONAL RESULTS

We now turn to a more detailed discussion of our results along the two cuts displayed in Fig. 2. With the parameter  $e$  defined as  $e \equiv s_x - s_y$ , these two cuts through the phase diagram correspond to  $e = 0.0$  and  $e = 0.3$ . The overview presented in Fig. 3 shows the fugacity de-

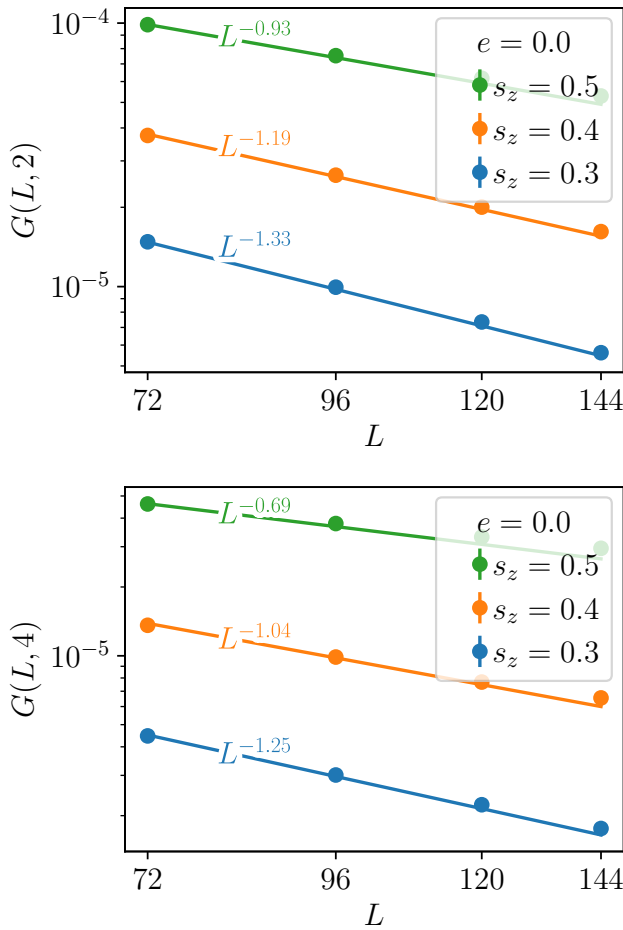


FIG. 8:  $G(L, 2)$  (top) and  $G(L, 4)$  (bottom) as a function of  $L$  on the  $e = 0$  cut for  $s_z \in [0.3, 0.5]$ .

pendence of the different components of the layering order parameter at a fixed size  $L = 72$ . To pinpoint the transition from one phase to another, and study in more detail the phases themselves, it is of course necessary to study the  $L$  dependence of  $\langle \mathcal{L}_\mu^2 \rangle$  as well as the Binder ratios corresponding to these order parameters. Here, we present some representative results of such a study.

Along the  $e = 0$  cut, we have  $s_x = s_y = (3 - s_z)/2$ . Fig. 6 shows the  $L$  dependence of the transverse columnar order parameter  $\langle \mathcal{C}_x^2 + \mathcal{C}_y^2 \rangle$  and the transverse layering order parameter  $\langle \mathcal{L}_x^2 + \mathcal{L}_y^2 \rangle$  for various  $s_z$  in the vicinity of the transition from the  $z$  layered phase to the sublattice ordered phase. Both of these can both be used to distinguish between these two phases, with both tending to zero in the thermodynamic limit in the  $z$  layered phase, and both tending to nonzero thermodynamic limits in the sublattice ordered phase.

These order parameters also identify an interesting aspect of the  $z$  layered phase, namely the presence of power-law order in the transverse columnar order parameter and the transverse layering order parameter. This is readily seen from the power-law fall off  $\sim 1/L^{\eta_{3d}}$  of these quan-

tities at large  $L$ , with  $1 < \eta_{3d} < 2$  and varying smoothly with  $s_z$  within the layered phase. To explore this further, we have quantified the strength of two-dimensional columnar order within each occupied bilayer by measuring  $G(L)$  as well as the connected correlation function  $g(r)$  evaluated at  $L/a$ , where  $a = 4$ . As is clear from Fig. 7, within each bilayer, there are critical correlations corresponding to two-dimensional power-law columnar order within each occupied bilayer, with exponent  $\eta_{2d}(0)$  that varies continuously with  $s_z$ .

If the two-dimensional columnar order parameters of different occupied bilayers had only been coupled to each other via weak correlations decaying exponentially with increasing  $\Delta z$ , the measured  $\eta_{3d}$  would have satisfied the equality  $\eta_{3d} = 1 + \eta_{2d}(0)$ . To explore this possibility, we have also measured  $G(L, \Delta z)$  for small nonzero  $\Delta z$ , which probes the correlation between the two-dimensional columnar order parameters of two occupied bilayers separated by  $\Delta z$  in the layering direction. From Fig. 8 which shows the  $L$  dependence of  $G(L, \Delta z)$  for nonzero  $\Delta z$  at various  $s_z$ , we see that this quantity also decays as a power law with increasing  $L$ , with exponent  $\eta_{2d}(\Delta z)$ . This is consistent with the fact that the measured  $\eta_{3d}$  and  $\eta_{2d}(0)$  always satisfy  $\eta_{3d} < 1 + \eta_{2d}(0)$  instead of the equality mentioned above. These transverse power-law correlations point to the unusual and interesting nature of this layered phase, which is discussed in more detail in Sec. V.

To obtain a more precise estimate of the location of the transition between this  $z$  layered phase and the sublattice ordered phase along the  $e = 0$  cut, we monitor the  $s_z$  dependence of corresponding Binder ratios of these transverse order parameters for various sizes  $L$ . A conventional second order critical point between the  $z$  layered phase and the sublattice ordered phase is expected to yield a crossing of the Binder ratio curves corresponding to different sizes  $L$ , whereas a first order transition is expected to lead to non-monotonic behaviour of these curves near the transition. As is clear from Fig. 9, we see neither of these behaviors. Instead, the Binder ratios for different sizes seem to stick together for  $s_z \lesssim 0.535$ , and splay apart for  $s_z \gtrsim 0.535$ .

This sticking of the Binder ratio curves corresponding to different  $L$  is what one expects in a critical phase, consistent with our earlier observation of power-law decay of the transverse layering and columnar order parameters as a function of system size  $L$  in the  $z$  layered phase. Further, the behavior of the Binder ratios in Fig. 9 is reminiscent of the stick and splay behavior of the Binder of the columnar order parameter in the vicinity of the transition between long-range columnar order and power-law columnar order in the two-dimensional fully-packed lattice gas of hard squares and dimers. All of this points to the fact that the  $z$  layered phase studied along this cut is indeed a critical phase. Finally, a direct confirmation of the sublattice ordering is also obtained from the  $L$  dependence of the  $\langle \omega^2 \rangle$ , which goes to zero with increasing  $L$  in the  $z$  layered phase but remains nonzero in the ther-

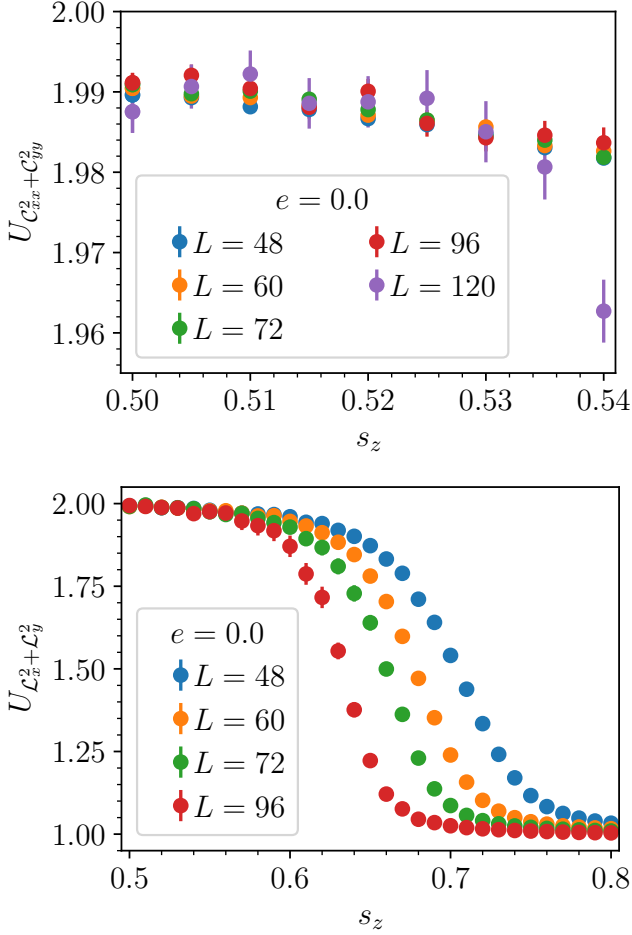


FIG. 9:  $U_{C_{xx}^2 + C_{yy}^2}$  (top) and  $U_{L_x^2 + L_y^2}$  (bottom) as a function of  $s_z$  on the  $e = 0$  cut across the  $z$  layered to sublattice order transition for various  $L$ .

mododynamic limit in the sublattice ordered phase, as seen in Fig. 10.

As  $s_z$  is increased further along the  $e = 0$  cut, the sublattice ordered phase terminates in a transition to  $z$  columnar order, which breaks lattice translation symmetry in the  $x$  and  $y$  directions, but has full lattice translation symmetry in the  $z$  direction. This is clear from examining the behaviour of  $\langle \mathcal{L}_z^2 \rangle$  and the corresponding Binder cumulant. Since the  $Z_2$  symmetry of lattice translations in the  $z$  direction is restored upon crossing this transition, while translation symmetry in other directions remains broken on either side of the transition, one expects this transition to be in the three dimensional Ising universality class. Indeed, as is clear from Fig. 11 results for the Binder ratio and its scaling collapse in the vicinity of this transition, our results are entirely consistent with this expectation.

Along the  $e = 0.3$  cut, we have  $s_x = s_y + 0.3$ ,  $s_y = (2.7 - s_z)/2$ . As we increase  $s_z$  along this cut, we go from the  $z$  layered phase first to an  $x$  columnar phase, which has two-fold symmetry breaking of lattice translations in

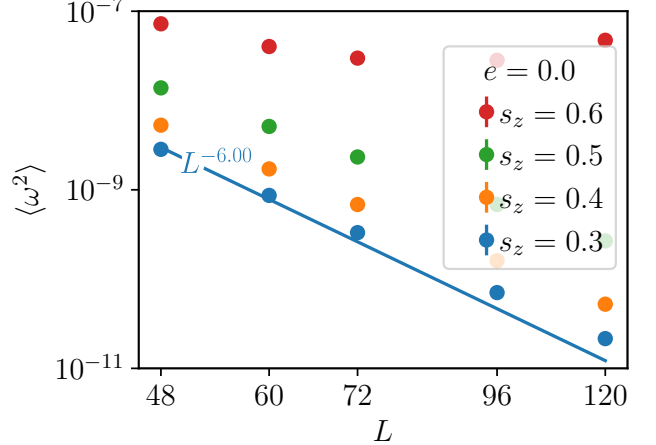


FIG. 10:  $\langle \mathcal{L}_z^2 \rangle$  as a function of  $L$  on the  $e = 0$  cut across the  $z$  layered to sublattice order transition for  $s_z \in [0.3, 0.6]$ . Note that  $\langle \mathcal{L}_z^2 \rangle$  falls off with  $L$  somewhat slower than  $1/L^6$  due to the presence of transverse power-law order within the occupied bilayers.

the  $y$  and  $z$  directions, while preserving lattice translation symmetry in the  $x$  direction. This is apparent from the  $L$  dependence of  $\langle \mathcal{L}_x^2 \rangle$  and  $\langle \mathcal{L}_y^2 \rangle$ , as shown in Fig. 12. A more precise estimate of the critical value of  $s_z$  is obtained from the stick and splay behavior of the corresponding Binder ratios, as shown in Fig. 13.

As  $s_z$  is increased further along this  $e = 0.3$  cut, there is a transition from the  $x$  columnar phase to the sublattice ordered phase. Again, one expects this transition to be in the Ising universality class since the two phases differ only by the  $Z_2$  symmetry breaking of lattice translations in the  $x$  direction. Our results are indeed consistent with this expectation. The same expectation is also borne out by our results for the next transition along this cut, at which the sublattice ordered phase gives way to the  $z$  columnar phase. This is clear from Fig. 14 which shows the corresponding crossing of the Binder ratios and their scaling collapse. For even larger values of  $s_z$  there is a second transition along this cut, to a  $z$  columnar phase, and finally, at still larger values of  $s_z$ , a transition to the  $y$  layered phase. We do not display our results for these transitions since they are entirely analogous to the results shown earlier for the transition between the  $x$  columnar phase and the sublattice ordered phase, and the transition between the  $z$  layered phase and the  $x$  columnar phase.

Unlike for the Ising transitions between the sublattice ordered phase and various columnar phases, we do not have a detailed understanding of the universality class of the transitions between the various layered phases and the sublattice ordered phase, and between the various layered phases and columnar phases. This is because of the unusual nature of the layered phase, which displays power-law transverse ordering, in the direction perpendicular to the layering direction. What is the correct

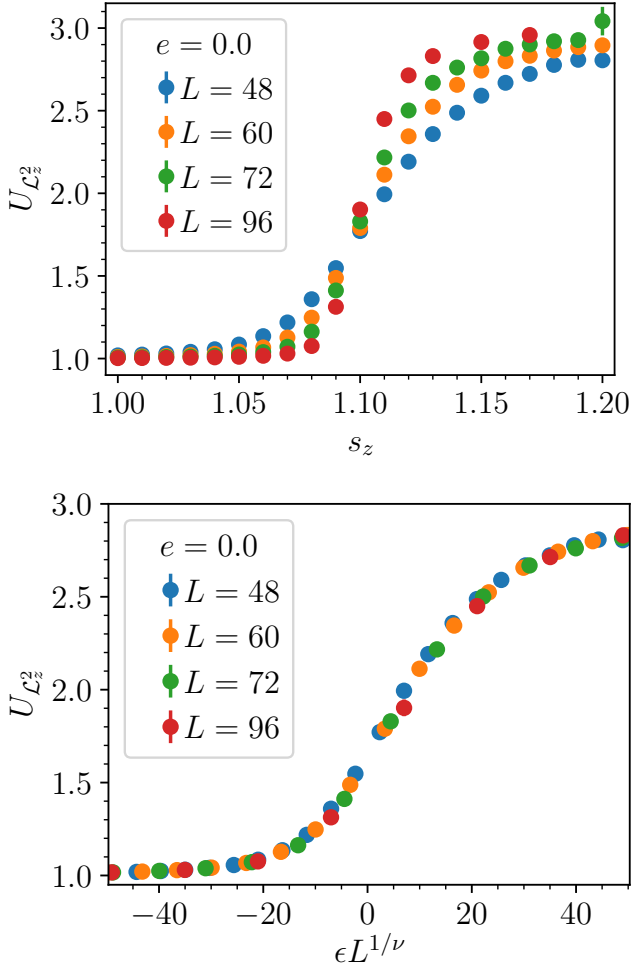


FIG. 11: (top)  $U_{L_z^2}$  as a function of  $s_z$  on  $e = 0$  cut across the sublattice order to  $z$  columnar transition for various  $L$ . (bottom) Scaling collapse of  $U_{L_z^2}$  as a function of  $\epsilon L^{1/\nu}$  with  $\epsilon = (s_z - 1.095)$  and  $\nu \approx 0.63$  of the 3D Ising universality class [21].

coarse-grained field-theoretical description of universal features of these continuous transitions? Although we are unable to answer this question, we note that the eventual answer would need to build on the answer to a related question: How can be understand the transverse power-law order of the layered phase itself within a coarse-grained effective field theory approach? Although our work does not fully answer this question either, the broad contours of an answer are sketched in the discussion below.

## V. POWER-LAWS IN THE LAYERED PHASE

Each occupied bilayer in the  $z$  layered phase is power-law ordered in the transverse directions, with power-law correlations of  $\mathcal{L}_x$  and  $\mathcal{L}_y$ . To understand this better,

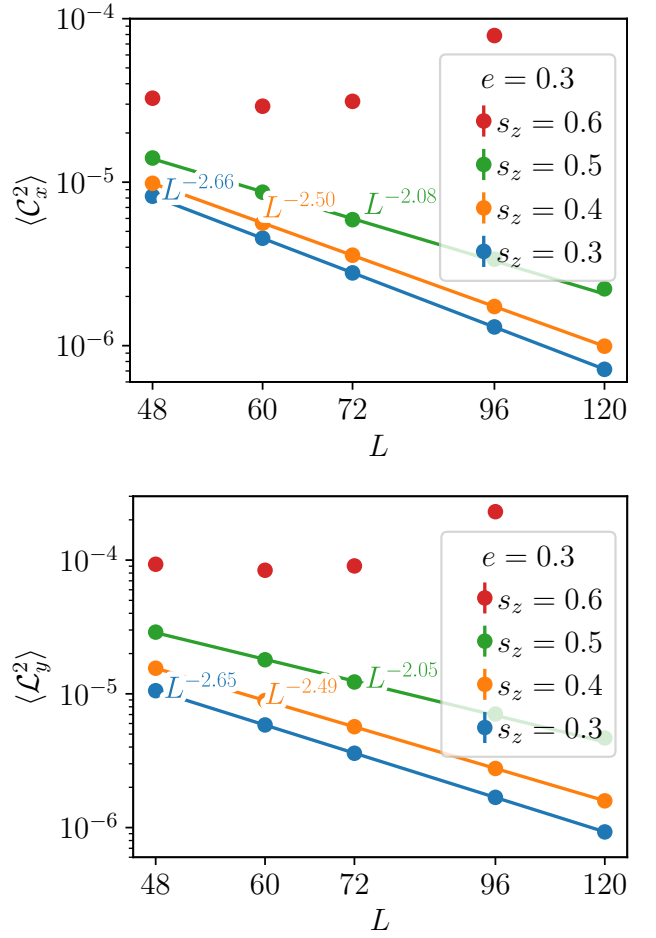


FIG. 12:  $\langle C_x^2 \rangle$  (top) and  $\langle L_y^2 \rangle$  (bottom) as a function of  $L$  on the  $e = 0.3$  cut across the  $z$  layered to  $x$  columnar transition for  $s_z \in [0.3, 0.6]$ .

we start in the  $s_z \rightarrow 0$  limit. When  $s_z = 0$ , there are only  $x$  and  $y$  plates present, and these clearly organize themselves into occupied bilayers separated from each other. Viewed along the  $z$  axis, each such occupied bilayer is seen to be equivalent to a fully-packed square lattice dimer model, with  $x$  plates represented by dimers along  $y$  links of the equivalent square lattice, and  $y$  plates represented by dimers along  $x$  links of this square lattice. The transverse power-law order of the occupied layers is simply understood in this limit as being a consequence of the power-law columnar order of the fully-packed dimer model on the square lattice. Thus, at  $s_z = 0$ , we expect power-law columnar order with power-law exponent  $\eta = 2$ .

As mentioned in the introduction, the power-law correlations of the fully-packed square lattice dimer model can be understood via a coarse-grained field theory whose action is written in terms of a fluctuating scalar height field that represents the electrostatic potential of a system of

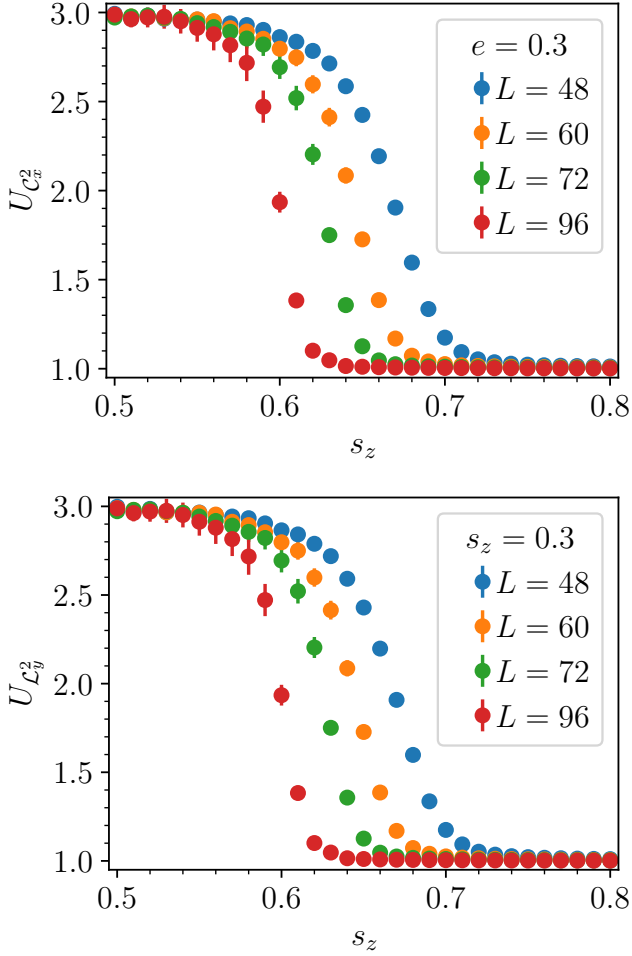


FIG. 13:  $U_{C_x^2}$  (top) and  $U_{L_y^2}$  (bottom) as a function of  $s_z$  on the  $e = 0.3$  cut across the  $z$  layered to  $x$  columnar transition for various  $L$ .

fluctuating dipoles:

$$S_{2d} = \pi g \int d^2r (\nabla_{\perp} h)^2, \\ Z \propto \int \mathcal{D}h \exp(-S), \quad (10)$$

with  $g = 1/2$ . In this description the local density of  $x$  dimers (which represent  $y$  plates) is given by  $(-1)^{x+y} \partial_y h + \mathcal{A}(-1)^x \cos(2\pi h)$ , while the local density of  $y$  dimers (which represent  $x$  plates) is given by  $(-1)^{x+y+1} \partial_x h + \mathcal{A}(-1)^y \sin(2\pi h)$ .

When  $s_z = \epsilon$ , with  $\epsilon > 0$  but very small,  $z$  plates are allowed. However, and this is key, the only configurations that contribute to the partition function in the thermodynamic limit have *pairs* of  $z$  plates, stacked one above the other in the  $z$  direction. When two such  $z$  plates are stacked one above the other in an occupied bilayer, they can be represented in the equivalent two dimensional system by a small admixture of hard squares introduced into the fully-packed square lattice dimer model. The fugac-

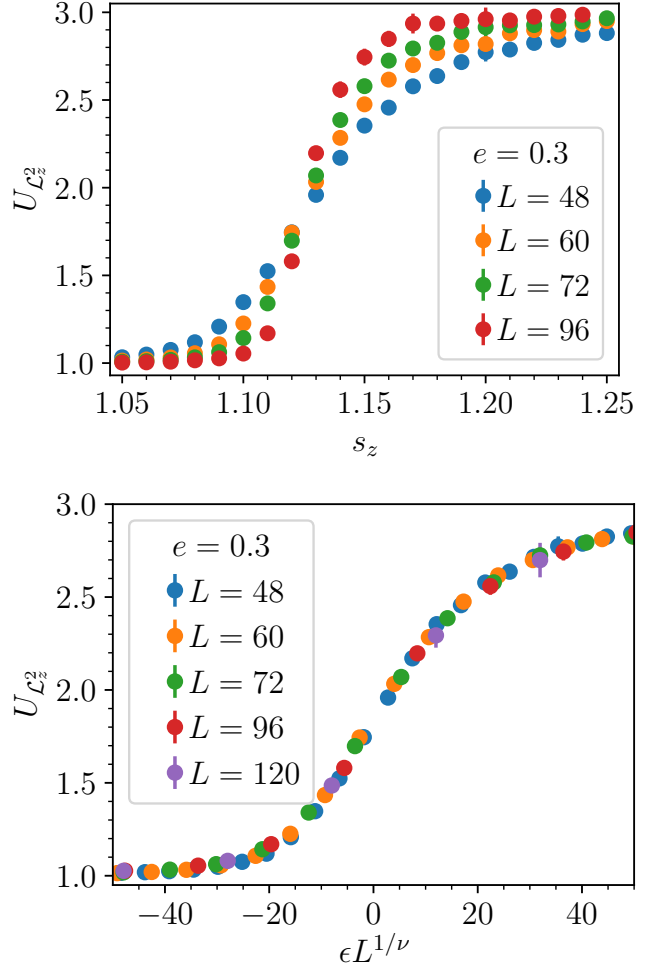


FIG. 14: (top)  $U_{L_z^2}$  as a function of  $s_z$  on  $e = 0.3$  cut across the sublattice order to  $z$  columnar transition for various  $L$ . (bottom) Scaling collapse of  $U_{L_z^2}$  as a function of  $\epsilon L^{1/\nu}$  with  $\epsilon = (s_z - 1.124)$  and  $\nu \approx 0.63$  of the 3D Ising universality class [21].

ity of these hard squares is of order  $\epsilon^2$ . This small density of hard squares increases the stiffness of the fluctuating height field, so that  $g(\epsilon) = 1/2 + \mathcal{O}(\epsilon^2)$ , leading to a decrease in the value of  $\eta$ , so that  $\eta = 2 - \mathcal{O}(\epsilon^2)$ .

If such a pair of  $z$  plates straddles two neighbouring occupied bilayers, it can be replaced by a *pair* of parallel  $x$  or  $y$  plates that straddle the two occupied bilayers. To  $\mathcal{O}(\epsilon^2)$ , these are the leading defects that destroy perfect layering and couple neighbouring occupied bilayers. Crucially, single  $x$  or  $y$  plates straddling neighbouring occupied bilayers do not contribute in the thermodynamic limit. Such plates can be viewed as a pair of holes in one layer of each of the two adjacent occupied bilayers. The full-packing constraint ensures that this pair of holes, which is a dipolar defect from the point of view of the equivalent problem of hard squares and dimers, cannot move on its own. In effect, the full-packing con-

straint ensures that these dipolar defects come in nearest-neighbour pairs. Thus, dipolar defects are confined into quadrupoles. This is very different from the purely two-dimensional problem of hard-squares and dimers. The fact that each occupied layer is actually part of a fully three-dimensional system is therefore crucial for understanding the nature of the defects, although our description is in terms of an equivalent two dimensional system.

We now argue that this confinement of the dipolar defects into quadrupoles is the reason that the power-law correlations within each occupied bilayer survive the coupling between neighbouring occupied bilayers. To see this, represent each occupied bilayer in the small  $\epsilon$  limit as a two-dimensional system of hard-squares and dimers. Ignoring the coupling between neighbouring occupied bilayers for the moment, this can be described by the effective action:

$$S_0 = \pi g \sum_z \int d^2r (\nabla_{\perp} h_z)^2. \quad (11)$$

The quadrupolar defects that couple the neighbouring occupied bilayers can then be represented by attractive interactions between one pair of parallel dimers in a layer and another such pair in the neighbouring layer. This leads to terms in the effective action that couple the height fields of neighbouring bilayers:

$$\begin{aligned} S &= S_0 + S_1 + S_2, \\ S_1 &= \lambda \sum_z \int d^2r [(\partial_x^2 h_z)(\partial_x^2 h_{z+1}) + (\partial_y^2 h_z)(\partial_y^2 h_{z+1})] + \\ &\quad + \lambda' \sum_z \int d^2r (\partial_{xy}^2 h_z)(\partial_{xy}^2 h_{z+1}), \\ S_2 &= \lambda'' \sum_z \int d^2r \cos(4\pi(h_z(r) - h_{z+1}(r))), \end{aligned} \quad (12)$$

with  $\lambda$ ,  $\lambda'$ , and  $\lambda''$  all vanishing in the  $\epsilon \rightarrow 0$  limit. Along the renormalization group (RG) fixed line with action  $S_0$  parameterized by  $g$ , all three perturbations that constitute  $S_1$  and  $S_2$  are seen to be *irrelevant* so long as  $8/g > 4$ , *i.e.*  $g < 2$ . The quadrupolar nature of the defects coupling neighbouring power-law correlated bilayers is now seen to be the key reason for the stability of these power-law correlated bilayers at nonzero  $s_z$ : In the absence of the constraints that force the dipolar defects to be confined into quadrupoles, a cosine term of the form  $\cos(2\pi(h_z(r) - h_z(r+1)))$ , representing a *single*  $x$  or  $y$  plate straddling two neighbouring occupied bilayers, would have been allowed. This term is relevant unless  $2/g > 4$ , *i.e.*  $g < 1/2$ , which is never the case since a small  $\mathcal{O}(\epsilon)$  value of  $s_z$  is already expected to *increase* the value  $g$  from  $g = 1/2$  to  $g = 1/2 + \mathcal{O}(\epsilon^2)$ .

Thus, the transverse power-law correlations in this layered phase are stabilized by constraints imposed by full-packing, which confine dipolar interlayer defects into quadrupoles. The effective field theory ideas that capture

this effect provide a natural explanation of the power-law correlations within each occupied bilayers. It should be possible to develop this analysis further, in order to also describe the nature of the correlations between two different occupied bilayers separated by a distance  $\Delta z$  in the layering direction. It would be interesting to pursue this further, and develop a theory for the relationship between the intra-layer power-law correlation exponent and the power-law exponent characterizing the  $L$  dependence of the three-dimensional transverse layering order parameter  $\langle \mathcal{L}_x^2 + \mathcal{L}_y^2 \rangle$ .

Finally, we note that the mechanism that stabilizes this critical phase is reminiscent of the basic physics of so-called “fractonic phases” that has received a great deal of attention in the literature [22–25] namely, constraints on the existence and mobility of isolated defects carrying some generalized charge. Does this similarity extend to the behaviour of vacancies introduced into this fully-packed system? This is one of the questions that motivates our parallel study of the hard plate lattice gas away from full packing.

## VI. ACKNOWLEDGEMENTS

We acknowledge useful discussions with R. Dandekar, R. Moessner, K. Ramola, and N. Shannon. GR gratefully acknowledges technical assistance from K. Ghadially and A. Salve of the Department of Theoretical Physics (DTP) of the Tata Institute of Fundamental Research (TIFR) and from the Scientific Computing and Data Analysis section of the Okinawa Institute of Science and Technology (OIST). A major portion of the results presented here formed part of the Ph.D thesis submission of GR to the TIFR Deemed University (2019), and was made possible by the generous allocation of computational resources made by DTP TIFR. The final stages of this work were facilitated by extensive computational resources provided by OIST. GR was supported by a graduate fellowship of the TIFR during a major part of this work, and by the TQM unit at the Okinawa Institute of Science and Technology during the final stages of this work. The work of SB was supported by a postdoctoral fellowship of the DTP TIFR. DM was supported by a graduate fellowship of the Institute of Mathematical Sciences (IMSc). KD was supported at the TIFR by DAE, India and in part by a J.C. Bose Fellowship (JCB/2020/000047) of SERB, DST India, and by the Infosys-Chandrasekharan Random Geometry Center (TIFR). DD’s work was partially supported by Grant No. DST-SR- S2/JCB-24/2005 of the Government of India.

*Author contributions* GR performed the computational work with assistance from DM. KD, RR, and DD conceived the project, directed the computational work, and finalized the manuscript using detailed inputs from GR. SB performed exploratory simulations in the preliminary stages of the work.

---

[1] J. Villain, R. Bidaux, J. P. Carton, and R. Conte, “Order as an effect of disorder,” *J. Phys. France* **41**, 1263–1272 (1980).

[2] C. L. Henley, “The “coulomb phase” in frustrated systems,” *Ann. Rev. of Cond. Mat. Phys.* **1**, 179–210 (2010).

[3] R. W. Youngblood and J. D. Axe, “Polarization fluctuations in ferroelectric models,” *Phys. Rev. B* **23**, 232–238 (1981).

[4] R. Youngblood, J. D. Axe, and B. M. McCoy, “Correlations in ice-rule ferroelectrics,” *Phys. Rev. B* **21**, 5212–5220 (1980).

[5] S. Papanikolaou, E. Luijten, and E. Fradkin, “Quantum criticality, lines of fixed points, and phase separation in doped two-dimensional quantum dimer models,” *Phys. Rev. B* **76**, 134514 (2007).

[6] F. Alet, Y. Ikhlef, J. L. Jacobsen, G. Misguich, and V. Pasquier, “Classical dimers with aligning interactions on the square lattice,” *Phys. Rev. E* **74**, 041124 (2006).

[7] P. Patil, I. Dasgupta, and K. Damle, “Resonating valence-bond physics on the honeycomb lattice,” *Phys. Rev. B* **90**, 245121 (2014).

[8] N. Desai, S. Pujari, and K. Damle, “Bilayer coulomb phase of two-dimensional dimer models: Absence of power-law columnar order,” *Phys. Rev. E* **103**, 042136 (2021).

[9] G. Rakala, K. Damle, and D. Dhar, “Fractional brownian motion of worms in worm algorithms for frustrated ising magnets,” *Phys. Rev. E* **103**, 062101 (2021).

[10] D. A. Huse, W. Krauth, R. Moessner, and S. L. Sondhi, “Coulomb and liquid dimer models in three dimensions,” *Phys. Rev. Lett.* **91**, 167004 (2003).

[11] C. Xu and C. Wu, “Resonating plaquette phases in SU(4) heisenberg antiferromagnet,” *Phys. Rev. B* **77**, 134449 (2008).

[12] A. F. Albuquerque and F. Alet, “Critical correlations for short-range valence-bond wave functions on the square lattice,” *Phys. Rev. B* **82**, 180408 (2010).

[13] Y. Tang, A. W. Sandvik, and C. L. Henley, “Properties of resonating-valence-bond spin liquids and critical dimer models,” *Phys. Rev. B* **84**, 174427 (2011).

[14] K. Damle, D. Dhar, and K. Ramola, “Resonating valence bond wave functions and classical interacting dimer models,” *Phys. Rev. Lett.* **108**, 247216 (2012).

[15] S. Pankov, R. Moessner, and S. L. Sondhi, “Resonating singlet valence plaquettes,” *Phys. Rev. B* **76**, 104436 (2007).

[16] D. Mandal, G. Rakala, N. Vigneshwar, K. Damle, D. Dhar, and R. Rajesh, “Vacancy driven phase transitions in a system of hard plates on a cubic lattice,” (In preperation).

[17] O. F. Syljuåsen and A. W. Sandvik, “Quantum monte carlo with directed loops,” *Phys. Rev. E* **66**, 046701 (2002).

[18] K. Ramola, K. Damle, and D. Dhar, “Columnar order and Ashkin-Teller criticality in mixtures of hard squares and dimers,” *Phys. Rev. Lett.* **114**, 190601 (2015).

[19] W. Krauth and R. Moessner, “Pocket Monte-Carlo algorithm for classical doped dimer models,” *Physical Review B* **67**, 064503 (2003).

[20] C. Domb, M. S. Green, and J. L. Lebowitz, *Phase Transitions and Critical Phenomena*, Phase Transitions and Critical Phenomena No. 3 (Academic Press, 1972).

[21] A. Pelissetto and E. Vicari, “Critical phenomena and renormalization-group theory,” *Phys. Rep.* **368**, 549–727 (2002).

[22] C. Xu and M. P. A. Fisher, “Bond algebraic liquid phase in strongly correlated multiflavor cold atom systems,” *Phys. Rev. B* **75**, 104428 (2007).

[23] M. Pretko, “Subdimensional particle structure of higher rank U(1) spin liquids,” *Phys. Rev. B* **95**, 115139 (2017).

[24] Y. You, Z. Bi, and M. Pretko, “Emergent fractons and algebraic quantum liquid from plaquette melting transitions,” *Phys. Rev. Res.* **2**, 013162 (2020).

[25] Y. You and R. Moessner, “Fractonic plaquette-dimer liquid beyond renormalization,” *arXiv preprint arXiv:2106.07664* (2021).